Incommensurate antiferromagnetism induced by a charge density wave in the cubic phase of $TbGe_{2.85}$

A. V. Tsvyashchenko,[1,2,*] D. A. Salamatin,[1,3] V. A. Sidorov,[1] A. E. Petrova,[1] L. N. Fomicheva,[1] S. E. Kichanov,[4] A. V. Salamatin,[5] A. Velichkov,[5,6] D. R. Kozlenko,[4] A. V. Nikolaev,[2,3] G. K. Ryasny,[2] O. L. Makarova,[7] D. Menzel,[8] and M. Budzynski[9]

[1]*Vereshchagin Institute for High Pressure Physics, RAS, 142190, Moscow, Troitsk, Russia*
[2]*Skobeltsyn Institute of Nuclear Physics Lomonosov Moscow State University, Leninskie gory, Moscow 119991, Russia*
[3]*Department of Problems of Physics and Energetics, Moscow Institute of Physics and Technology, 141700 Dolgoprudny, Russia*
[4]*Frank Laboratory of Neutron Physics, Joint Institute for Nuclear Research, Dubna, P.O. Box 79, Moscow, Russia*
[5]*Dzelepov Laboratory of Nuclear Problems, Joint Institute for Nuclear Research, Dubna, P.O. Box 79, Moscow, Russia*
[6]*Institute for Nuclear Research and Nuclear Energy, 1784 Sofia, Bulgaria*
[7]*Kurchatov's complex of NBICS-technologies, National Research Center "Kurchatov Institute", 123182 Moscow, Russia*
[8]*Institute of Condensed Matter Physics, TU Braunschweig, 30816 Braunschweig, Germany*
[9]*Institute of Physics, M. Curie-Sklodowska University, 20-031 Lublin, Poland*

(Received 24 June 2015; revised manuscript received 24 August 2015; published 23 September 2015)

Temperature dependencies of the electrical resistivity, magnetic susceptibility, and heat capacity have been obtained in the cubic phase of $TbGe_{2.85}$ (the $AuCu_3$ structure), synthesized at high pressure. The macroscopic measurements indicate that a charge density wave is formed below 145 K and an antiferromagnetic ordering is realized below 19 K. Hyperfine interaction data obtained with the time differential perturbed angular correlation method with ^{111}Cd probes inserted in the $TbGe_{2.85}$ lattice suggest that the charge density wave is incommensurate in the temperature region 19–145 K, but becomes commensurate below 19 K. The neutron diffraction reveals a complex antiferromagnetic spiral structure in the magnetically ordered phase. We discuss relations between the charge density wave and helical ordering in $TbGe_{2.85}$ and $TbPd_3$.

DOI: 10.1103/PhysRevB.92.104426 PACS number(s): 71.45.Lr, 75.25.−j, 62.50.−p, 61.05.Qr

I. INTRODUCTION

It has long been known that a one-dimensional metal is inherently unstable with respect to charge or spin-density waves [1–3]. Such instability, called Peierls instability, in one-dimensional materials is often accompanied by the formation of a charge density wave (CDW). Although our understanding of the microscopic mechanism of CDW formation is incomplete, simple models suggest that the low dimensionality produces anisotropic Fermi surfaces with regions of low curvature and high density of electron states, which favor a CDW through the "nesting" mechanism. Since in the three-dimensional case (3D) cubic intermetallic compounds are usually isotropic, the likelihood of a CDW state is significantly diminished, and the nesting mechanism leads to a CDW only in a limited number of materials [4].

The cubic phase of $TbGe_{2.85}$ studied in the present work is a rare example of such a compound. We will show that the formation of CDW which sets in at 145 K influences almost all its physical properties including an antiferromagnetic transition at a still lower temperature of 19 K. The cubic phase of $TbGe_{2.85}$ is metastable at normal conditions and can be synthesized only at high pressures. The crystal structure is of the $AuCu_3$ type with the $Pm\bar{3}m$ space group (group number 221). Earlier, cubic phases of $YbGe_{2.85}$, $TbGe_{2.85}$, and $DyGe_{2.85}$ of the same $AuCu_3$ structure have been obtained and investigated by the nuclear method of time-dependent perturbed angular $\gamma\,\gamma$ correlations (TDPAC) working on probe ^{111}Cd nuclei inserted at vacancies of the germanium sublattice at high temperatures (77–300 K) [5]. TDPAC spectroscopy examines the local electric field gradient (EFG) and magnetic field at the ^{111}Cd probe nucleus, which contain important information on the physical properties of these compounds. In particular, the pressure dependence of the characteristic quadrupolar frequency ν_Q in $YbGe_{2.85}$ indicates that the valence of Yb changes from 2.46 to 2.89 with external pressure increasing from zero to 8 GPa [5]. Unlike macroscopic techniques that measure averaged quantities such as magnetization, resistivity, etc., TDPAC is a microscopic method that can determine local variations of magnetic moment and exchange. In the present work, we apply the TDPAC spectroscopy and neutron diffraction to the study of the cubic phase of $TbGe_{2.85}$.

It is worth noting that at normal conditions the stoichiometric compound $TbGe_3$ crystallizes in another structure, which is the orthorhombic base-centered one with the space group $Cmcm$ (group 63) [6]. At temperatures below $T_N = 40$ K, it undergoes a transition to a magnetically ordered phase. The magnetic ordering is different above and below the characteristic temperature $T_{ic} = 24$ K. In the temperature range $T_{ic} < T < T_N$, the magnetic structure is of complex nature (incommensurate with multiple q vectors) and coexists with the paramagnetic phase. Below T_{ic}, the magnetic structure becomes commensurate with two Tb sublattices coupled antiferromagnetically.

II. EXPERIMENT

Polycrystalline samples of $TbGe_{2.85}$, $TbGe_3$, and $TbPd_3$ were synthesized at a pressure of 8 GPa as described in Ref. [7]. High pressure was produced in the device of "toroid" type [8].

*tsvyash@hppi.troitsk.ru

For synthesis we used a mixture of Tb (chemical purity 99.9%) and Ge (chemical purity 99.999%) or Pd (chemical purity 99.99%). The crystal structure of samples was examined by x-ray diffraction (XRD). Measurements were performed at room temperature with the diffractometer STOE IPDS-II using Mo-K_α radiation. Data on magnetization were obtained using a SQUID magnetometer. Measurements of the heat capacity were carried out with a Quantum Design PPMS instrument. The electric resistance was measured by the standard four contact method (details are given in Ref. [9]).

The parameters of hyperfine interactions in the TDPAC method were obtained with radioactive ^{111}In/^{111}Cd nuclei as nuclear probes. The parent isotope ^{111}In with high specific activity was obtained using the ^{109}Ag(α,2n) ^{111}In reaction by irradiating a silver foil in the 32 MeV α beam at the Nuclear Physics Institute cyclotron (Moscow State University). Nuclear ^{111}In/^{111}Cd probes were inserted in the $TbGe_{2.85}$ lattice under high pressure and temperature [10]. The ^{111}In half-life is 2.83 d. The intermediate 245 keV state has a spin $I = 5/2$, electric quadrupole moment $Q = +0.83(13)$ b, g factor $g_N = -0.306$, and a half-life of 85 ns [11]. The precession of quadrupolar and magnetic moments of the intermediate 245 keV state in $TbGe_{2.85}$ was registered by means of the time anisotropy of the $\gamma\,\gamma$ cascade 171–245 keV.

Angle correlations are characterized by the perturbation factor $G_{kk}(t)$ ($k = 2, 4, \ldots$). The time anisotropy function $R(t)$ is related with the perturbation factor $G_{22}(t)$, $R(t) = -A_{22}Q_2G_{22}(t)$, where $Q_2 \approx 0.80$ is the solid-angle correction [12], and $A_{22} = -0.18$ is the unperturbed angular correlation coefficient. The function $R(t)$ is measured by recording the delayed coincidence spectra $N(\pi/2,t)$ and $N(\pi,t)$ at time t and at angles $\pi/2$ and π between detectors: $R(t) = -2[N(\pi,t) - N(\pi/2,t)]/[N(\pi,t) + 2N(\pi/2,t)]$. The TDPAC measurements were carried out using a four-detector spectrometer [13]. For low temperatures, we used an optical four-window cryostat JANIS (model SHI-950-5). Experimental data were processed with the DEPACK program [14].

Neutron powder diffraction measurements were recorded at room and $T = 10$ K temperatures on the DN-12 diffractometer [15] at the IBR-2 high-flux pulsed reactor (FLNP JINR, Dubna, Russia). Diffraction patterns were collected at scattering angle $2\Theta = 90^\circ$ and 45.5° with resolutions $\Delta d/d \sim 0.015$ and 0.022, correspondingly. The low temperature was achieved with a closed-cycle helium cryostat. The exposition time for a one pattern record was about 2 hours. Neutron diffraction patterns were analyzed with the Rietveld method using the FULLPROF program [16].

III. RESULTS

A. Macroscopic measurements

Powder x-ray diffraction has confirmed that all samples of $TbGe_{2.85}$ are cubic (the $AuCu_3$ type) with the space group $Pm\bar{3}m$ and the lattice parameter consistent with the literature data [5] ($a = 4.287(4)$ Å at room temperture). The $AuCu_3$ structure can be viewed as a framework of Ge_6 octahedra sharing corners with the large Tb atoms in the interstitials between octahedra. In contrast to $TbGe_{2.85}$, stoichiometric samples of $TbGe_3$, along with the cubic fraction contain 10% of the orthorhombic phase stable at normal conditions.

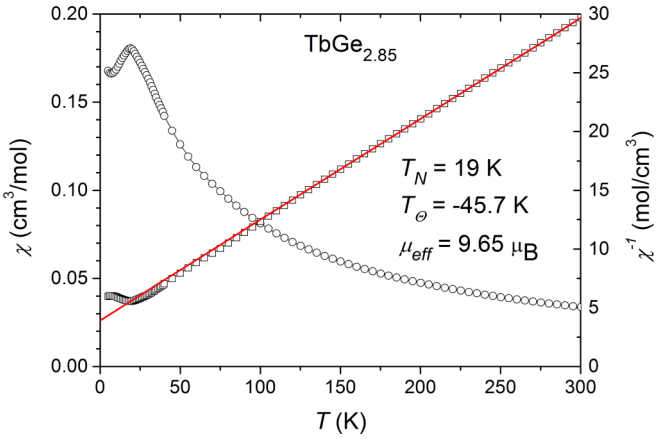

FIG. 1. (Color online) χ and χ^{-1} as a function of temperature in the range 2–300 K for $TbGe_{2.85}$.

The magnetic susceptibility χ and the inverse susceptibility $1/\chi(T)$ of $TbGe_{2.85}$ measured at normal pressure in the temperature range from 2 to 300 K are shown in Fig. 1. The plot for χ clearly demonstrates a characteristic peculiarity at $T_N = 19$ K, indicating an antiferromagnetic ordering below this temperature. From the χ^{-1} dependence, we find the Curie-Weiss temperature $\Theta = -46$ K and the effective magnetic moment $\mu_{\rm eff} = 9.65\ \mu_B$/f.u. consistent with the trivalent configuration of the Tb^{3+} free ion ($\mu = 9.72\ \mu_B$). The difference between the inverse susceptibilities, i.e., $\chi^{-1} - \chi_{\rm CW}^{-1}$, where χ refers to experimental data and $\chi_{\rm CW}$ to the Curie-Weiss law, plotted in Fig. 2 as a function of temperature, however, clearly demonstarates that χ deviates from the Curie-Weiss law below the characteristic temperature $T_{\rm CDW} = 145$ K.

Temperature dependencies of electric resistivity for $TbGe_{2.85}$ and $TbGe_3$ are shown in Fig. 3. For $TbGe_{2.85}$, we reproduce two resistivity plots measured at normal pressure and $P = 0.9$ GPa. One sees that the typical metallic linear dependence of resistivity observed at high temperatures in

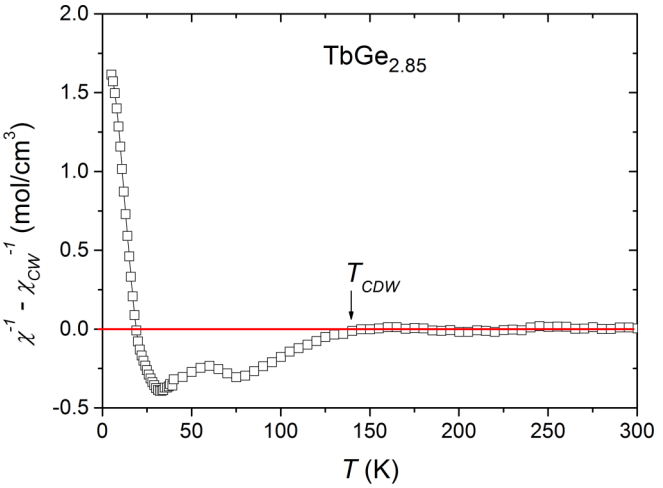

FIG. 2. (Color online) Difference between the experimental data for χ^{-1} and the Curie-Weiss fit ($\chi_{\rm CW}^{-1}$) for $TbGe_{2.85}$.

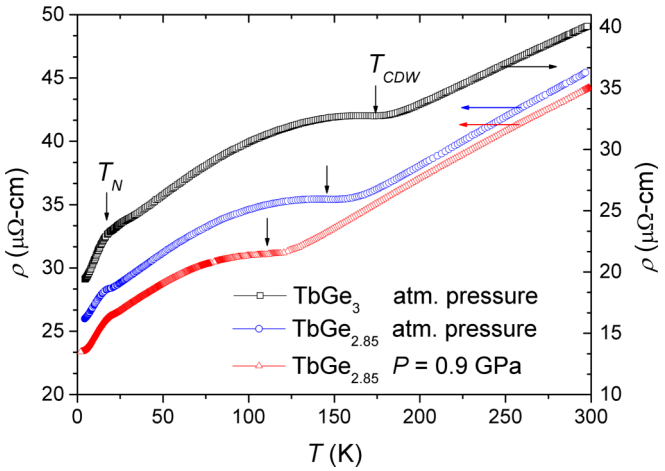

FIG. 3. (Color online) Resistivity of $TbGe_3$ and $TbGe_{2.85}$ vs temperature. The red and blue dots represent data for $TbGe_{2.85}$ for different external pressures (see text for details), while the black dots for $TbGe_3$.

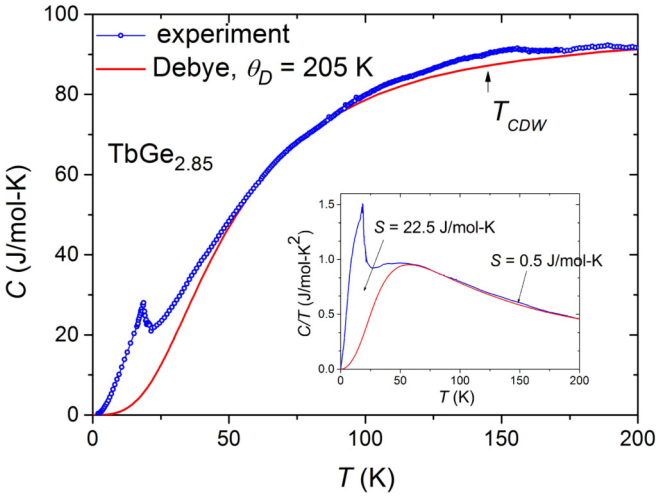

FIG. 4. (Color online) Heat capacity vs temperature (blue dots) and Debyes law approximation with $\Theta_D = 205$ K (red line). (Inset) C/T vs T.

all plots below a certain temperature T_{CDW} (marked by short vertical arrow) demonstrates a humplike peculiarity with a flat region around T_{CDW}. Conventionally, the peak in the curve of logarithmic derivative of electrical resistivity ($\ln \rho$) with respect to reciprocal temperature $1/T$, i.e., $d[\ln \rho(T)]/d(1/T)$ versus T, is used to define the character temperature of the Peierls transition [17]. By applying the same method, we determined the transition temperatures T_{CDW}, as shown in Fig. 3. Inspection of Fig. 3 reveals that T_{CDW} decreases with pressure (compare two plots for $TbGe_{2.85}$) and increases with decreasing of the number of vacancies (compare plots for $TbGe_{2.85}$ and $TbGe_3$). High sensitivity of T_{CDW} to any (anisotropic) changes in the lattice parameters of the material, for example, to external pressure or vacancies is usually considered as a result of electron-phonon interactions and Fermi surface nesting [17,18]. With further temperature lowering, the T_{CDW} plateau in all plots is replaced with a rapid drop of electric resistivity. Notice, however, that the peculiarity related with the antiferromagnetic ordering is observed at the same temperature $T_N = 19$ K in all plots indicating that the Néel temperature is independent of the number of defects.

Heat capacity of $TbGe_{2.85}$ at atmospheric pressure is given in Fig. 4 (blue dots). The experimental data have been approximated by Debyes law (red line) with Debyes temperature $\Theta_D = 205$ K. Comparison between the two plots reveals two regions of discrepancy. First region corresponds to temperatures around T_{CDW} (shown also by arrow in Fig. 4), while the second to low temperatures around T_N. At T_N, we observe the λ anomaly, which once again points out to the antiferromagnetic ordering. The excess (above the Debye law) values of heat capacity at T_{CDW} and T_N are $\triangle C_{CDW} = 2.26$ J/mol K and $\triangle C_N = 21.95$ J/mol K, correspondingly. By integrating the temperature dependence of C/T around T_{CDW} (see the inset of Fig. 4), we find that the entropy change at the CDW transition is 0.5 J/mol K. The total magnetic entropy change is $\triangle S = 22.5$ J/mol K, which agrees well with the value of $R \ln(2J + 1) = 21.33$ J/mol K for the free Tb^{3+} ion having $J = 6$.

We thus conclude that the high-temperature T_{CDW} anomaly clearly and consistently manifests itself in plots of electric resistance and heat capacity. Also, the temperature dependence of the magnetic susceptibility starts to deviate from the Curie-Weiss law below T_{CDW}. Moreover, the character of the temperature peculiarity in heat capacity and electric resistivity data allows us to identify T_{CDW} as the onset of the formation of a charge density wave. The jump in heat capacity $\triangle C_{CDW} = 2.26$ J/mol K and the entropy change $\triangle S = 0.5$ J/mol K associated with the CDW transition, are very close to that found in the cubic compound $La_3Co_4Sn_{13}$, which exhibits a CDW transition at 152 K [19].

B. TDPAC (local) measurements

Earlier, we have shown that probed ions $^{111}In/^{111}Cd$ inserted in $TbGe_{2.85}$ occupy germanium lattice sites [5]. Inserted $^{111}In/^{111}Cd$ ions keep the host site $4/mmm$ point symmetry, which being lower than the cubic symmetry, allows for nonzero electric field gradient (EFG) V_{zz} [20,21] with the gradient asymmetry parameter $\eta = (V_{xx} - V_{yy})/V_{zz} = 0$. The resultant TDPAC spectra $R(t)$ from the $^{111}In/^{111}Cd$ probes in $TbGe_{2.85}$ measured at temperatures 30-300 K and normal pressure are given in Fig. 5.

At room temperature (upper panels of Fig. 5), the spectrum is consistent with the single quadrupolar frequency $\nu_Q = 37.5(5)$ MHz [EFG $V_{zz} = h\nu_Q/eQ = 1.87(3)\ 10^{17}$ V/sm^2] and $\eta = 0.2(1)$. The obtained quadrupole frequency is in agreement with the value of ν_Q reported in Ref. [5]. The refined value of η differs from zero probably due to Ge vacancies present in the lattice. At $T = 50$ K, the best fit is obtained with the single quadrupolar frequency $\nu_Q = 41(1)$ MHz and $\eta = 0.25(2)$. From the Fourier transformation of spectra we notice a broadening of frequency distribution at temperatures below 160 K (see Fig. 5). The temperature evolution of the quadrupolar frequency ν_Q is shown in Fig. 6. There are two very different dependencies: with temperatures above and below T_N. The antiferromagnetic region ($T < T_N$) will be discussed later. In the paramagnetic phase ($T > T_N$), ν_Q

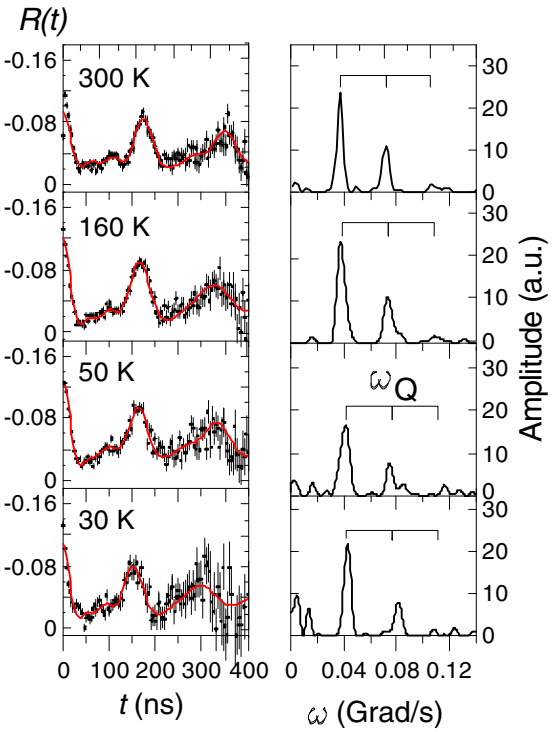

FIG. 5. (Color online) TDPAC spectra of ^{111}Cd probes in $TbGe_{2.85}$ in the temperature range 30–300 K. Left panels give the angular anisotropic functions $R(t)$ and their fits, right panels represent Fourier transforms of $R(t)$ with resolved quadrupolar frequencies.

increases with temperature lowering with the slope -0.015 ± 0.002 MHz/K obtained from the 22–300 K data interpolation. Such behavior of ν_Q is typical for f-electron compounds in the magnetically disordered phase [22,23].

Below the Néel temperature T_N, the magnetic moments of terbium order and the conduction electrons become polarized. This results in a polarization of the probe spin density, leading to a nonzero magnetic field at ^{111}In/^{111}Cd nuclei. As a result, the ^{111}In/^{111}Cd probes experience both hyperfine magnetic and

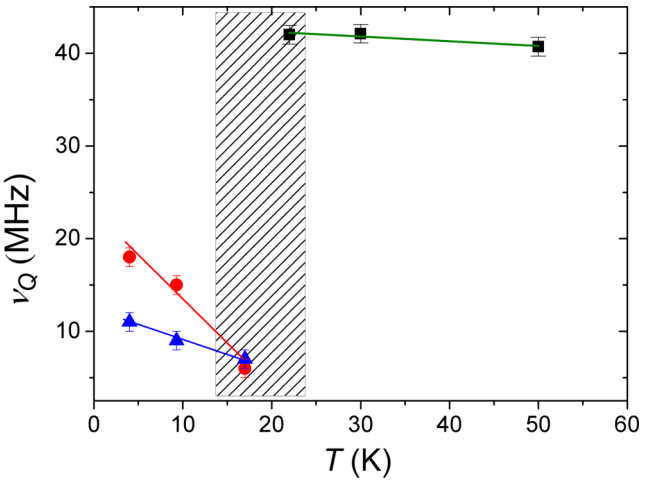

FIG. 6. (Color online) The quadrupole frequency ν_Q as a function of temperature in the range 4–50 K. The hatched interval marks the onset of antiferromagnetic-paramagnetic transition.

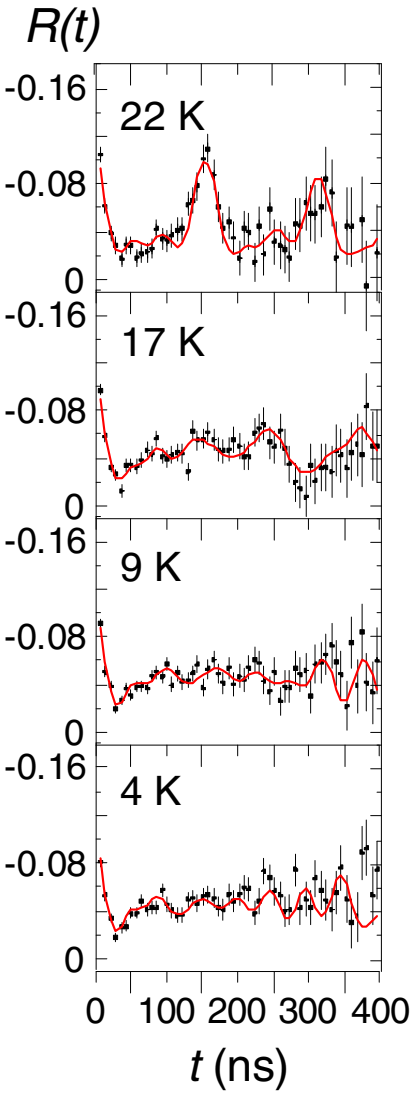

FIG. 7. (Color online) TDPAC spectra $R(t)$ of ^{111}Cd probes in $TbGe_{2.85}$ and their fits (red lines) in the temperature range 4–22 K.

electric quadrupole interactions. The corresponding TDPAC spectra of $TbGe_{2.85}$ in the antiferromagnetic phase are given in Fig. 7.

Clearly, the spectra are very different from those in the paramagnetic phase (compare with Fig. 5). In particular, the 4 K spectrum has been fit with two quadrupolar frequencies $\nu_{Q1} = 18(1)$, $\nu_{Q2} = 11(1)$ MHz and two Larmor precession frequencies $\nu_{L1} = 6(1)$, $\nu_{L2} = 10(1)$ MHz at ^{111}In/^{111}Cd nuclei. Two Larmor precession frequencies correspond to the hyperfine magnetic fields $B_{hf1} = h\nu_L/g\mu_N = 2.6(4)$ T and $B_{hf2} = 4.3(4)$ T. These two distinct sets of frequencies and fields are due to signals from two nonequivalent probe ions. From the TDPAC spectrum, we obtain that their occupation ratio is approximately 1:2. Two hyperfine magnetic fields appear to be almost temperature independent, while the quadrupolar frequencies ν_{Q1} and ν_{Q2} decrease with temperature rising albeit with different rate and at 17 K, in the vicinity of the transition to the magnetically disordered phase, become equal, i.e., $\nu_{Q1} \approx \nu_{Q2} = 7(1)$ MHz. The situation is

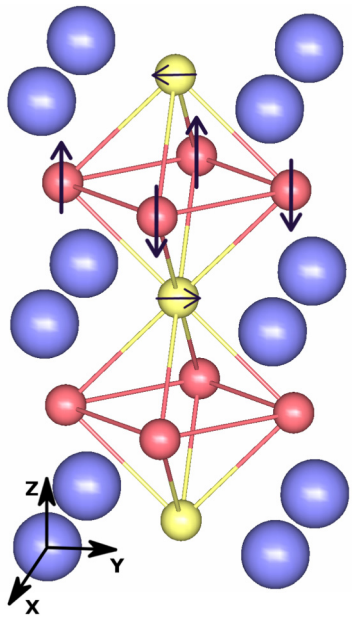

FIG. 8. (Color online) Crystallographic structure of $TbGe_{2.85}$ in the antiferromagnetic state with magnetically and electronically nonequivalent Ge sites. Large spheres represent Tb atoms, small spheres Ge atoms. Electronically nonequivalent Ge sites are shown by different colors, magnetically nonequivalent by different arrows.

illustrated in Fig. 6. The evolution of hyperfine magnetic fields indicates that formerly equivalent germanium sites (i.e., above T_N) become magnetically nonequivalent below T_N, Fig. 8. Electronic nonequivalence also sets in below T_N in the form of two distinct quadrupole frequencies and increases with temperature lowering, Fig. 6. At 22 K, the quadrupole frequency changes discontinuously to the paramagnetic value. Such a suppression of quadrupolar frequency at the magnetic ordering has been observed earlier in Laves phases AFe_2 (A = Zr, Y, Lu) [24].

Frequency broadening observable for TDPAC spectra below $T_{CDW} = 145$ K and the existence of only one quadrupole frequency indicate that the charge density wave formed below T_{CDW} is incommensurate, i.e., it is characterized by a propagation vector, which is incommensurate in respect to the $TbGe_{2.85}$ crystal lattice. The appearance of two distinct quadrupole frequencies below T_N allows us to suggest that the magnetic ordering is accompanied by a transition from incommensurate to commensurate CDW structure [25,26].

C. Neutron diffraction

To further refine the magnetic order in the low-temperature phase, we have performed neutron diffraction of $TbGe_{2.85}$ samples. Diffraction patterns have been measured at two temperatures: 10 K (below T_N) and room temperature. The room-temperature powder diffraction pattern given in Fig. 9 has confirmed the $Pm\bar{3}m$ cubic structure ($a = 4.287$ Å) resolved earlier by x-ray diffraction data [5]. Figure 10 shows the 10-K neutron diffraction pattern obtained in the magnetically ordered phase of $TbGe_{2.85}$. First, no change of the cubic structure has been detected [$a = 4.280(2)$ Å at 10 K] and no magnetic contributions to nuclear peaks have

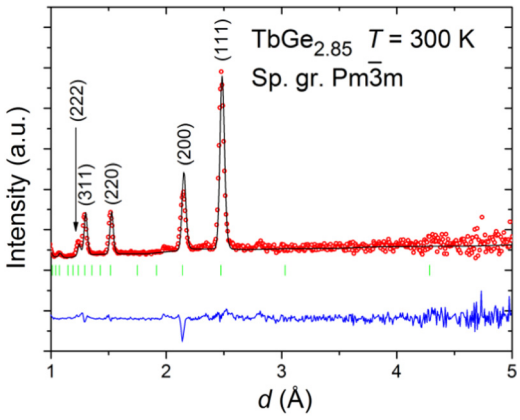

FIG. 9. (Color online) Refined neutron powder diffraction pattern of $TbGe_{2.85}$ at 300 K.

been found. Secondly, the appearance of numerous magnetic superlattice Bragg peaks [see Fig. 10] at this temperature indicates a complicated antiferromagnetic ordering. The best fit to the 10-K neutron pattern has been achieved for the incommensurate antiferromagnetic spiral spin configuration of Tb sublattice with the propagation vector $k = 2\pi/a(0.5,0,\xi_z)$, where $\xi_z = 0.160(1)$. The spiral period of this structure is 26.8 Å and the magnetic moment of Tb ions is 7.8(5) μ_B. No magnetic reflections from the germanium sublattice have been detected probably because of the smallness of the induced polarization. Note that the ^{111}Cd-TDPAC method also finds that the induced spin polarization of the germanium sublattice is quite small.

IV. DISCUSSION

Earlier, we have suggested a two-stage scenario of phase transformations in $TbGe_{2.85}$: (1) CDW formation at 145 K with incommensurate propagation vector, which persists down to the temperature $T_N = 19$ K, (2) antiferromagnetic ordering at T_N, below which the CDW becomes commensurate. Unfortunately, in the literature there are no examples of CDW formation in compounds with the $AuCu_3$ cubic structure. In the absence of detailed theoretical consideration, we cannot

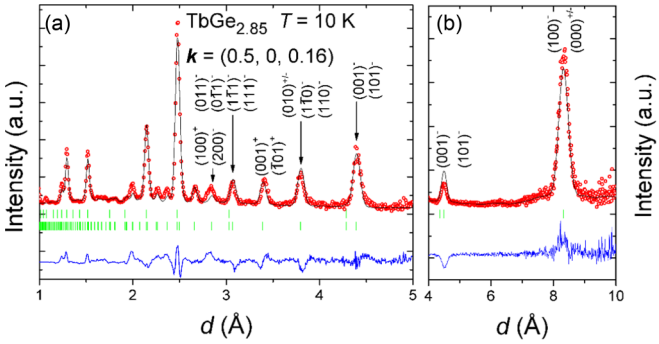

FIG. 10. (Color online) Refined neutron powder diffraction pattern of $TbGe_{2.85}$ obtained at 10 K in the magnetically ordered state. (a) Data for $1 < d < 5$ and (b) data for $4 < d < 10$. The (0,0,1) and (1,0,1) peaks are shown in both panels for comparison of their intensities.

describe fully the nature of CDW in $TbGe_{2.85}$. Nevertheless, CDW has been detected in a number of other cubic structures. For example, in cubic Laves structures, CDW has been found in superconductors ZrV_2 and HfV_2 [27], where its formation was related with the nesting of Fermi surface with vector $q \parallel [100]$. In the cubic compound $Sr_3Ir_4Sn_{13}$, the formation of CDW was accompanied with a structural phase transition and doubling of the lattice constant [28]. It has been shown that the Fermi surface of $Sr_3Ir_4Sn_{13}$ has small curvature regions, which apparently favors the nesting mechanism [28]. Nesting also gives rise to CDW in CuV_2S_4 with a cubic spinel structure [29]. In the last two examples, lowering of space symmetry takes place below the CDW formation temperature.

On the other hand, numerous germanium lattice vacancies in $TbGe_{2.85}$ can play a considerable role in CDW formation. In Ref. [30], it has been shown that point defects could act as nucleation centers for CDW, forming pinned CDW domains separated by atomically abrupt charge boundaries. From this point of view, the dependence of T_{CDW} on the number of vacancies deduced from the temperature plots of electric resistivity (Fig. 3) is consistent with the CDW pinning mechanism in $TbGe_{2.85}$ [31]. Notice that the application of high pressure on $TbGe_{2.85}$ suppresses the CDW formation temperature, Fig. 3. It is also worth noting that in the orthorhombic base-centered structure of the stoichiometric compound $TbGe_3$ in the absence of germanium vacancies, no CDW has been reported [6]. There, however, an incommensurate to commensurate sequence in magnetic ordering takes place [6].

We believe that the formation of CDW in the cubic phase of $TbGe_{2.85}$ gives rise to a spiral antiferromagnetic spin structure in the ordered state. Modulated atomic displacements, which most likely occur along the [001] direction, are consistent with the nonzero anisotropic gradient parameter η and lead to a local (hidden) loss of the inversion center and appearance of the antisymmetric Dzyaloshinskii-Moria exchange interaction [32–34]. This interaction in turn stabilizes the spiral structure of terbium magnetic moments.

For a better understanding of physical mechanisms in $TbGe_{2.85}$, we have synthesized and studied $TbPd_3$ [35], which to the best of our knowledge is the only cubic compound with the same $AuCu_3$ structure and incommensurate magnetic ordering at T_N. (The Néel temperature varies in the range 2.5–4 K depending on the experimental measurements.) The magnetic order in $TbPd_3$ is very complicated and the authors of Ref. [35] give two possible structures: helical or sinusoidally modulated arrangement of the ordered magnetic moments with the wave vector $\vec{k}_1$ for the Tb sublattice and $\vec{k}_2$ for the induce magnetism of the Pd sublattice. It has been found that the induced moments of Pd are relatively large [35]. Note that an induced magnetic ordering exists also in $TbGe_{2.85}$, although the small values of hyperfine magnetic fields in two magnetically nonequivalent germanium sites indicate that their magnetic moments are small. This is the main reason why the induced magnetic order is not visible in neutron diffraction, see Fig. 10. However, TDPAC spectra and theoretical analysis of Ref. [23] permit us to identify their arrangement [$\mu_1(B_{hf1})$ and $\mu_2(B_{hf2})$] as orthogonal-antiferromagnetic with the wave vector $\vec{k}$ of the Tb sublattice. Such nontrivial magnetic behavior of both compounds raises a question on possible similarities between them including a CDW formation. CDW is observed

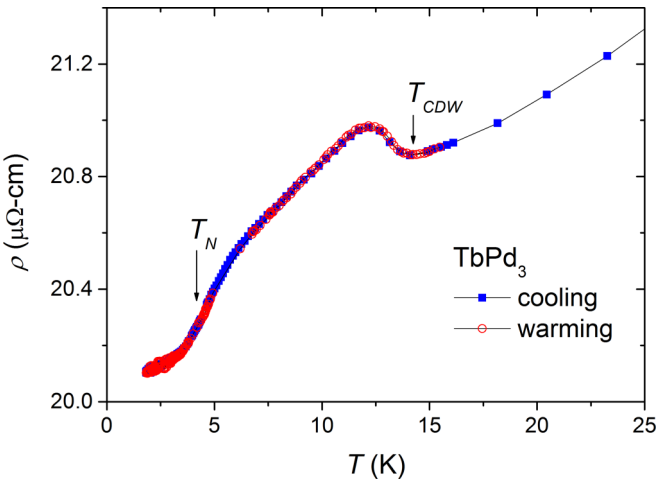

FIG. 11. (Color online) Temperature dependence of the resistivity of $TbPd_3$.

in $TbGe_{2.85}$, but so far no experimental evidence has been given for the existence of CDW in $TbPd_3$. To clarify this question, we have synthesized $TbPd_3$ [the $AuCu_3$ cubic structure, $a = 4.090(6)$ Å] and measured its electric resistivity, shown in Fig. 11. One clearly sees two anomalies: the first is at the temperature $T_{CDW} = 14.3$ K, and the second is at $T_N = 4.3$ K. The second peculiarity related with the onset of the antiferromagnetic ordering, is in agreement with data of Ref. [35]. The T_{CDW} anomaly in $TbPd_3$ represents a steep rise of resistivity, which is expected to occur when CDW is formed. This supports our conclusion on the significant role of CDW in formation of spiral magnetic structures in centrosymmetric cubic compounds.

V. CONCLUSIONS

We have synthesized the cubic phase (the $AuCu_3$ structure) of $TbGe_{2.85}$ at high pressure and measured its magnetic susceptibility, electric resistivity, heat capacity, and TDPAC spectra from the $^{111}In/^{111}Cd$ nuclear probes inserted in sites of the germanium sublattice, Figs. 1–7. In addition, neutron diffraction measurements at 300 and 10 K have been performed, see Figs. 9 and 10, respectively. We have observed a charge density wave formation at the temperature $T_{CDW} = 145$ K and antiferromagnetic ordering to spiral structure at $T_N = 19$ K. From TDPAC data analysis, it follows that CDW is incommensurate above T_N but becomes commensurate below this temperature. In the magnetically ordered phase, we have resolved two nonequivalent arrangements of induced magnetic moments of ^{111}Cd probes. The two hyperfine fields, $B_{hf1} = 2.6(4)$ T and $B_{hf2} = 4.3(4)$ T, are orthogonal to each other with the 1 : 2 probe occupation ratio. The magnetic diffraction peaks have been indexed with a propagation vector $k = 2\pi/a(0.5,0,0.160)$ indicating an incommensurate antiferromagnetic helimagnetic structure. To confirm the relation between CDW and spiral magnetic order in centrosymmetric cubic compounds, we have measured the temperature dependence of resistivity for $TbPd_3$, which is crystallized in the same $AuCu_3$ structure and undergoes a transition to an incommensurate magnetic phase at $T_N = 4.3$ K. The resistivity plot (Fig. 11) for $TbPd_3$ clearly

demonstrates the charge density wave anomaly at $T_{CDW} = 14.3$ K. From our data we conclude that CDW can lead to a hidden symmetry lowering with suppression of the inversion symmetry and appearance of the magnetic antisymmetric Dzyaloshinskii-Moriya interaction. In the future, we plan a more detailed study of $TbGe_{2.85}$ aiming at the relation between the CDW suppression by pressure and magnetic ordering. Also, the hidden symmetry lowering in $TbGe_{2.85}$ should be further investigated at low temperature by refinement of its crystallographic structure.

ACKNOWLEDGMENTS

The authors are grateful to S. M. Stishov, D. V. Tonev, V. B. Brudanin, and N. G. Chechenin, for support of this work. The work was supported by the Russian Foundation for Basic Research (Grant No. 14-02-00001), the Russian Science Foundation (Grant RSF-14-22-00093), and by special programs of the Department of Physical Science, Russian Academy of Sciences. The work at the Joint Institute for Nuclear Research was carried out under the auspices of a Polish representative in the JINR.

[1] R. E. Peierls, in *Quantum Theory of Solids* (Oxford University Press, Oxford, England, 1955), p. 108.
[2] H. Frohlich, Proc. Roy. Soc., Ser. A **223**, 296 (1954).
[3] A. W. Overhauser, Phys. Rev. Lett. **4**, 462 (1960).
[4] R. M. Fleming, F. J. DiSalvo, R. J. Cava, and J. V. Waszczak, Phys. Rev. B **24**, 2850 (1981).
[5] A. V. Tsvyashchenko, A. I. Velichkov, A. V. Salamatin, L. N. Fomicheva, D. A. Salamatin, G. K. Ryasny, A. V. Nikolaev, M. Budzynski, R. A. Sadykov, and A. V. Spasskiy, J. Alloys Compd. **552**, 190 (2013).
[6] P. Schobinger-Papamatellos, J. Rodriguez-Carvajal, and K. H. J. Buschow, J. Phys.: Condens. Matter **19**, 236201 (2007).
[7] A. V. Tsvyashchenko, J. Less-Common Met. **99**, L9 (1984).
[8] L. G. Khvostantsev, L. F. Vereshchagin, and A. P. Novikov, High Temp.-High Press. **9**, 637 (1977).
[9] A. E. Petrova, V. A. Sidorov, and S. M. Stishov, Physica B: Condens. Matter **359-361**, 1463 (2005).
[10] A. V. Tsvyashchenko, L. N. Fomicheva, A. A. Sorokin, G. K. Ryasny, B. A. Komissarova, L. G. Shpinkova, K. V. Klementiev, A. V. Kuznetsov, A. P. Menushenkov, V. N. Trofimov, A. E. Primenko, and R. Cortes, Phys. Rev. B **65**, 174513 (2002).
[11] P. Herzog, K. Freitag, M. Reuschenbach, and H. Walitzki, Z. Phys. A **294**, 13 (1980).
[12] R. M. Steffen and H. Frauenfelder, in *Perturbed Angular Correlations*, edited by E. Karlsson, E. Matthias, and K. Siegbahn (North-Holland, Amsterdam, 1964).
[13] V. B. Brudanin, D. V. Flossofov, O. I. Kochetov, N. A. Korolev, M. Milanov, V. Ostrovskiy, V. N. Pavlov, A. V. Salamatin, V. V. Timkin, A. I. Velichkov, L. N. Fomicheva, A. V. Tsvyashchenko, and Z. Z. Akselrod, Nucl. Instrum. Methods Phys. Res. A **547**, 389 (2005).
[14] B. Lindgren, DEPACK—an interactive data analyses program, University of Uppsala, Institute of Physics Report, UUIP-1017, 1980, https://getinfo.de/en/search/id/TIBKAT%3A562271279/.
[15] V. L. Aksenov, A. M. Balagurov, V. P. Glazkov, D. P. Kozlenko, I. V. Naumov, B. N. Savenko, D. V. Sheptyakov, V. A. Somenkov, A. P. Bulkin, V. A. Kudryashev, and V. A. Trounov, Physica B **265**, 258 (1999).
[16] J. Rodriguez-Carvajal, Physica B **192**, 55 (1993).
[17] G. Gruner, *Density Waves in Solids* (Addison-Wesley, Reading, MA, 1994).
[18] S. L. Budko, T. A. Wiener, R. A. Ribeiro, P. C. Canfield, Y. Lee, T. Vogt, and A. H. Lacerda, Phys. Rev. B **73**, 184111 (2006).
[19] H. F. Liu, C. N. Kuo, C. S. Lue, K.-Z. Syu, and Y. K. Kuo, Phys. Rev. B **88**, 115113 (2013).
[20] G. P. Schwartz and D. A. Shirley, Hyperfine Interact. **3**, 67 (1977).
[21] S. J. Asadabadi, S. Cottenier, H. Akbarzadeh, R. Saki, and M. Rots, Phys. Rev. B **66**, 195103 (2002).
[22] S. Jalali Asadabadia and H. Akbarzadehb, Physica B **349**, 76 (2004).
[23] S. Demuynck, L. Sandratskii, S. Cottenier, J. Meersschaut, and M. Rots, J. Phys.: Condens. Matter **12**, 4629 (2000).
[24] L. G. Shpinkova and A. A. Sorokin, Phys. Stat. Sol. (b) **147**, K77 (1988).
[25] T. Butz, A. Vasquez, H. Ernst, and A. Lerf, Phys. Lett. A **58**, 51 (1976).
[26] T. Butz, A. Vasquez, H. Saitovitch, G. M. Kalvius, and A. Lerf, Hyperfine Interact. **4**, 798 (1978).
[27] F. Chu, T. E. Mitchell, S. P. Chen, M. Šob, R. Siegl, and D. P. Pope, MRS Proc. **364**, 1389 (1994).
[28] L. E. Klintberg, S. K. Goh, P. L. Alireza, P. J. Saines, D. A. Tompsett, P. W. Logg, J. Yang, B. Chen, K. Yoshimura, and F. M. Grosche, Phys. Rev. Lett. **109**, 237008 (2012).
[29] J. Matsuno, A. Fujimori, L. F. Mattheiss, R. Endoh, and S. Nagata, Phys. Rev. B **64**, 115116 (2001).
[30] H. H. Weitering, J. M. Carpinelli, A. V. Melechko, J. Zhang, M. Bartowiak, and E. W. Plummer, Science **285**, 2107 (1999).
[31] S. V. Zaitsev-Zotov, Phys. Usp. **47**, 533 (2004).
[32] I. Dzyaloshinski, J. Phys. Chem. Solids **4**, 241 (1958).
[33] T. Moriya, Phys. Rev. **120**, 91 (1960).
[34] P. Bak and M. H. Jensen, J. Phys. C **13**, L881 (1980).
[35] O. Elsenhans, P. Fischer, A. Furrer, K. N. Clausen, H. G. Purwins, and F. Hulliger, Z. Phys. B: Condens. Matter **82**, 61 (1991).